Regular Article

PHYSICAL CHEMISTRY RESEARCH
Published by the
Iranian Chemical Society
www.physchemres.org
info@physchemres.org

Phys. Chem. Res., Vol. 13, No. 1, 69-76, March 2025
DOI: 10.22036/pcr.2024.470263.2558

Effects of Support Type on Stability of Nickel Catalysts in a Fixed-bed Reactor: Deactivation Modeling Using Hybrid ANN/GPLE Approaches

M. Ghofran Pakdel[a], S.H. Zohdi[a,*], A.A. Mirzaei[b] and H. Atashi[a]

[a]*Department of Chemical Engineering, Faculty of Engineering, University of Sistan and Baluchestan, P.O. Box: 98164-161, Zahedan, Iran*
[b]*Department of Chemistry, Faculty of Sciences, University of Sistan and Baluchestan, Zahedan, Iran*
(Received 28 July 2024, Accepted 22 October 2024)

This paper used the neural network method to determine an appropriate deactivation model and the steady state activity. Using the wet impregnation method, the Nickel catalysts were prepared on the α-Al_2O_3, γ-Al_2O_3, SiO_2, and TiO_2 supports. The performances of catalysts were evaluated in a fixed bed reactor at constant conditions as follows: P = 20 bar, T = 583 K, and H_2/CO = 3. For the 20%Ni/TiO_2 catalyst, the second-order Generalized Power-Law Equation (GPLE) model and the other catalysts, the first-order GPLE model can predict the catalyst deactivation behavior well. A comparison of model parameters showed that the use of TiO_2 as support increased the long-term stability of nickel catalyst in the fixed bed reactor. XRD analysis demonstrated crystal growth on the supports and sintering deactivation mechanism.

Keywords: Catalyst deactivation, artificial neural network, GPLE models, steady-state activity, Industrial economy

INTRODUCTION

Growing energy demand due to the increasing world population, and international agreements to reduce greenhouse gas emissions from fossil fuels, boost the study of new energy sources [1,2]. Methanation ($CO+3H_2=CH_4+H_2O$) is an important chemical process in which CO_x converts to CH_4 through the hydrogenation reaction. It can purify the syngas used in the Fischer-Tropsch synthesis [3]. In Fischer-Tropsch reactions, activity and selectivity depend on the nature and support structure, metal loading, and catalyst preparation methods. A decrease in catalyst activity is an inevitable part of the catalytic processes that often occur due to fouling, coking, and poisoning caused by compounds present in the feed to the reactor [4]. Nickel and cobalt catalysts are widely used in the Fischer Tropsch synthesis and CO_2 methanation [5]. The values of operating conditions such as H_2/CO feed ratio and temperature in the methanation process are usually higher than Fischer Tropsch synthesis [6]. Nickel catalysts are highly effective in hydrogenation reactions, which can be beneficial for certain FTS processes. They are excellent for methanation, converting carbon monoxide and hydrogen into methane. Nickel is relatively inexpensive compared to other catalysts like cobalt and ruthenium. The high hydrogenation activity of nickel often leads to excessive methane production, which is not desirable when the goal is to produce longer-chain hydrocarbons. Nickel catalysts tend to produce fewer long-chain hydrocarbons compared to cobalt and iron catalysts [7]. Cobalt (Co) catalysts are highly active and selective for producing long-chain hydrocarbons, making them ideal for FTS. They exhibit good stability and resistance to deactivation, which is crucial for long-term operations. On the other hand, Cobalt is more expensive than nickel and iron, which can increase the overall cost of the process. Moreover, the presence of water can lead to catalyst deactivation, which is a significant drawback in FTS processes [7,8].

Iron (Fe) catalysts are versatile and can operate under a wide range of conditions, including high temperatures and pressures. Iron is abundant and inexpensive, making it a cost-effective option for FTS [9]. Iron catalysts are effective in producing olefins and alcohols, which are valuable chemical

*Corresponding author. E-mail: zohdi@eng.usb.ac.ir

feedstocks. Iron catalysts generally produce a broader range of hydrocarbons, including a significant amount of light hydrocarbons. Iron catalysts can suffer from deactivation due to carbon deposition and other factors.

Deactivation of nickel catalysts due to the sintering of nickel particles and coke deposition is one of the significant challenges for its commercial applications [10,11]. Much effort has been focused on the stability of the metal phase against sintering [12]. Recent studies showed that the sintering of active phases was affected by factors such as nature and support pores and strong interactions between support and metal [13,14]. In recent years, numerous additives have been used to improve metal dispersion and minimize coke formation [15-17]. Many researchers have investigated the formation and absorption of coke as a deactivation agent on a Ni/Al_2O_3 catalyst [18]. Barrientos *et al.* investigated the effects of promoters such as Zr, Mg, Br, and calcium oxide on the supported nickel catalyst and evaluated their resistance to coke formation under low-temperature methanation conditions [19]. Feyzi *et al.* studied the effect of sulfur on the catalytic behavior of $Fe\text{-}Ni/Al_2O_3$ in the conversion of synthesized gas to light olefins [20]. Olesen *et al.* studied the carbon formation, which deactivates the Ni/Al_2O_3 catalyst due to CO Methanation [21]. Wang *et al.* investigated the effect of carbon deposition on the long-term stability of Ni/SiO_2 catalyst in the methanation reaction [22]. Ni/Al_2O_3 catalyst with loading above 20% nickel has excellent thermal stability due to the dispersion of nickel particles on Al_2O_3 [23]. Dowlati *et al.* studied the deactivation behavior of $Co\text{-}Ni/TiO_2$ catalysts under industrial conditions for 300 hours [24]. Van de Loosdrecht *et al.* studied the effect of metal loading and reduction temperature on carbon deposition over Ni/SiO_2 and Ni/TiO_2 catalysts [25].

Artificial Neural Network (ANN) is known as an efficient approach for accurate data extrapolation and reduction of laboratory costs. Hence, applying ANN is economically advantageous for predicting the behavior of expensive industrial catalysts. Shiva *et al.* used a hybrid ANN/DOE methodology to study the lumped kinetic modeling of Fischer Tropsch synthesis on a Fe-Co/MgO catalyst [26]. Ghofran Pakdel *et al.* applied the artificial neural network approach to investigate the effect of nickel loading on the deactivation models of Ni/Al_2O_3 catalyst during the FTS [27].

Performing experiments for a long time is usually expensive and time-consuming. On the other hand, support has an essential role in the industrial catalytic processes. Artificial Neural Network is known as a promising technique for predicting the behaviors of experimental data. ANN can be used to extrapolate the activity data in the catalyst sciences. According to our literature reviews, there is no report about the effects of support on the catalyst stability and deactivation parameters. In this study, the impact of support type on the stability of the catalysts was investigated by studying the model parameters using an artificial neural network.

EXPERIMENTAL

Using the wet impregnation method, the nickel catalysts were prepared on the $\alpha\text{-}Al_2O_3$, $\gamma\text{-}Al_2O_3$, SiO_2, and TiO_2 supports. Before the impregnation, supports were dried at 393 K for 6 h and then calcined in air for 10 h at 773 K. The $\alpha\text{-}Al_2O_3$ support was prepared by calcining the $\gamma\text{-}Al_2O_3$ support in the air at 1373 K for 10 h. The supports were impregnated with an aqueous solution of $Ni(NO_3)_2.6H_2O$, then dried at 393 K for 3 h, and finally calcined in air at 723 K for 3 h. Before the experiments, catalyst reduction was performed for 4 h under atmospheric conditions, a gas flow rate of 450 Nml/min, and a temperature of 773 K. Then the temperature was cooled down to 583 K. Experiments were conducted at a feed ratio (H_2/CO) of 3 and GHSV of 75000-150000 Nml/h. Further details are provided in reference [28].

RESULTS AND DISCUSSIONS

Figure 1 presents the activity of $20\%Ni/SiO_2$, $20\%Ni/\alpha\text{-}Al_2O_3$, $20\%Ni/\gamma\text{-}Al_2O_3$, and $20\%Ni/TiO_2$ catalysts during the time of stream (TOS).

Catalyst Deactivation Models

The main criterion for calculating the catalyst deactivation is through the comparison of the activity of each run with the maximum conversion [29]. Equation (1) shows the percentage amount of activity drop during the reaction.

$$\text{Percentage of activity drop} = \frac{reaction\ rate\ at\ any\ time}{\text{initial reaction rate}} \times 100 \quad (1)$$

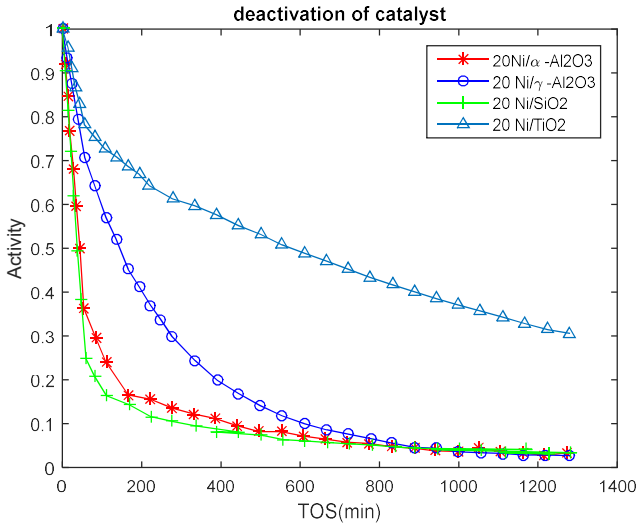


Fig. 1. Activity drop of the nickel catalysts in the presence of various supports (at a constant operating condition: P = 20 bar, T = 583 K, and $H_2/CO = 3$).

Deactivation models describe the stability behavior of a catalyst. These models play an important role in process control and reactor design.

Catalyst deactivation rate is defined as the rate of decreasing catalyst activity during a reaction time as follows:

$$-r_{deactive} = -\frac{da}{dt} \tag{2}$$

When the activity reaches a stable value, the form of deactivation is as follows.

$$-r_{deactive} = k_d (a - a_{\inf inite})^{\xi} \tag{3}$$

where ξ, k_d, and $a_{infinite}$ are deactivation order, deactivation constant, and long-time activity, respectively. If $\xi = 1$, then Eq. (2) converts to the first-order GPLE model.

$$\int_{a_0}^{a} \frac{da}{(a - a_{\inf inite})} = -\int_{t_0}^{t} k_d dt \rightarrow Ln(a - a_{\inf inite}) = -k_d t \rightarrow [Ln(a - a_{\inf inite}) - Ln(1 - a_{\inf inite})] = -k_d t \tag{4}$$

$$Ln\frac{a - a_{\inf inite}}{1 - a_{\inf inite}} = -k_d t \rightarrow \frac{a - a_{\inf inite}}{1 - a_{\inf inite}} = \exp(-k_d t) \rightarrow (a - a_{\inf inite}) = (1 - a_{\inf inite})\exp(-k_d t) \tag{5}$$

$$a = (1 - a_{\inf inite})\exp(-k_d t) + a_{\inf inite} \tag{6}$$

If $\xi = 2$, then Eq. (2) converts to the second-order GPLE model.

$$\frac{-da}{dt} = k_d (a - a_{\inf inite})^2 \rightarrow \frac{da}{(a - a_{\inf inite})^2} = -k_d dt \rightarrow \int_{a_0}^{a} \frac{da}{(a - a_{\inf inite})^2} = -\int k_d t \rightarrow -(a - a_{\inf inite})^{-1}\Big|_1^a = -k_d t \tag{7}$$

$$(a - a_{\inf inite})^{-1} - (1 - a_{\inf inite})^{-1} = k_d t \rightarrow (a - a_{\inf inite})^{-1} = k_d t + (1 - a_{\inf inite})^{-1} \rightarrow a - a_{\inf inite} = (k_d t + (1 - a_{\inf inite})^{-1})^{-1} \tag{8}$$

$$a = (k_d t + (1 - a_{\inf inite})^{-1})^{-1} + a_{\inf inite} \tag{9}$$

Artificial Neural Network

Evaluating the performance of the ANN simulation was performed by the regression analysis between the experimental data and the network outputs. The criteria used to determine network performance are:

1. Root Mean Square Error (RMSE)

$$RMSE = \sqrt{\frac{1}{N}\sum_{i=1}^{N}(a_i - p_i)^2} \tag{10}$$

2. Coefficient of determination (R squared)

$$R^2 = 1 - \left(\frac{\sum_{i=1}^{N}(a_i - p_i)^2}{\sum_{i=1}^{N} a_i^2}\right) \tag{11}$$

3. Coefficient of variation

$$C.V. = \frac{RMSE}{\sum_{i=1}^{N} a_i} * 100 \tag{12}$$

In the above equations, N represents the number of data, a_i, and p_i represent the actual and predicted data, respectively. The smaller the coefficient of variation (C.V.) and root mean square error (RMSE), and the closer the coefficient of determination (R^2) is to one, the better the network performance.

The lower the RMSE values, the better the inputs in the training set are trained, and the more accurate their responses are. However, it does not mean that the network will provide

better outputs for new inputs. In other words, a small RSME is not an apparent reason for the excellent performance of the network, and this is the case for the coefficient of determination (R^2) and the coefficient of variation (C.V.). Training data is not sufficient to judge the performance of the network and requires the application of new data and comparing the network outputs with the inputs.

Neural network performance for the catalysts. Table 1 shows the parameters of the artificial neural network for the Ni catalysts. Stopping the training step based on reaching the minimum error gradient for the 20%Ni/SiO_2 catalyst showed that the mean square error (MSE) was 7.2125×10^{-6} in the 84 training period. The μ (training factor) value at the end of the 84 training period and the amount of validation at the end of this training were 1×10^{-6} and 6, respectively. The best performance for the validation data in period 78 was 4.7641×10^{-6}. After 84 periods, the network error reached a certain level showing the convergence of the network.

For the 20%Ni/α-Al_2O_3 catalyst, the minimum error gradient over 36 training periods was 4.3814×10^{-5} for stopping the training step. The μ value at the end of the 36 training periods was 1×10^{-6}. Validation was also completed at the end of the 36 training period. In the 36 training stages of the network, the mean squared error for the best performance of the validation data in period 30 was 5.2323×10^{-6}. After 36 periods, the network error reached a certain level indicating the convergence of the network.

The best performance of the validation data for the 20%Ni/γ-Al_2O_3 catalyst was obtained in period 22 and the mean squared error was 8.0182×10^{-6}. After 22 periods, the network error reached a certain level indicating the convergence of the network. The minimum error gradient was achieved to 1.0553×10^{-5} in the 28 training period for stopping the training step. Data validation was also completed at the end of 28 training periods and the amount of μ at the end of this period was 1×10^{-7}.

For the 20%Ni/TiO_2 catalyst, the mean squared error in the 41st network training steps was 8.0347×10^{-6} in period 35 for the best performance of the validation data. After 35 periods, the network error reached a certain level that showed the convergence of the network. The training step was stopped based on achieving the minimum error gradient (1.5607×10^{-6}) over the 41st training period. The amount of μ at the end of the 41st training period was 1×10^{-10}. Validation has also been completed at the end of the 41 training period.

Table 1. Parameters of Artificial Neural Network for the Ni Catalysts

Catalyst	MSE	Training period	μ
20Ni/SiO_2	7.2125×10^{-6}	84	1×10^{-6}
20 Ni/ α -Al_2O_3	4.3814×10^{-5}	36	1×10^{-6}
20Ni/ γ -Al_2O_3	8.0182×10^{-6}	28	1.0553×10^{-5}
20Ni/TiO_2	8.0347×10^{-6}	35	1.5607×10^{-6}

Table 2. Comparing a_∞ Calculated Using GPLE (First and Second-order) Models and ANN for Model Determination

Catalyst	a_∞ (GPLE1)	a_∞ (GPLE2)	a_∞ (ANN)
20Ni/SiO_2	0.06	-0.004	0.03
20 Ni/ α -Al_2O_3	0.066	-0.009	0.03
20Ni/ γ -Al_2O_3	0.042	-0.133	0.02
20Ni/TiO_2	0.368	0.234	0.26

Interpretation of Deactivation Models

Table 2 shows the long-term activity (a_∞) of the supported Ni catalysts calculated using the GPLE1, GPLE2 models, and the ANN method. According to the results of the neural network extrapolation, a_∞ is 0.03 for the 20%Ni/SiO_2 and 20%Ni/α-Al_2O_3 catalysts. Furthermore, this parameter for the 20%Ni/γ-Al_2O_3 and 20%Ni/TiO_2 catalysts reaches 0.02 and 0.26, respectively. On the other hand, a_∞ obtained from the second-order GPLE model for the 20%Ni/SiO_2, 20%Ni/α-Al_2O_3, 20%Ni/γ-Al_2O_3, and 20%Ni/TiO_2 reach -0.004, -0.009, -0.133, and 0.234, respectively. Since the steady-state activity of a catalyst cannot be a negative number, the second-order GPLE model is rejected for the 20%Ni/SiO_2, 20%Ni/α-Al_2O_3, and 20%Ni/γ-Al_2O_3 catalysts. Whereas the values of

a_∞ obtained from the first-order GPLE models are positive for all the catalysts. Therefore, the GPLE1 model can sufficiently describe the stability behaviors of the 20%Ni/SiO_2, 20%Ni/α-Al_2O_3, and 20%Ni/γ-Al_2O_3 catalysts. This result is consistent with the previous research [27]. The long-term activity of the 20%Ni/TiO_2 catalyst obtained from the second-order GPLE model is closer to that obtained from ANN, so the GPLE2 model is preferable for this catalyst.

Table 3 presents the deactivation constant (k_d) for the nickel-supported catalysts. The regression analysis is based on the Levenberg-Marquardt algorithm that is the Least Square optimization method for solving nonlinear problems.

The higher the value of k_d, the faster a catalyst deactivates. By comparing the k_d parameters for the different supported nickel catalysts, it was found that the parameter value for the 20%Ni/TiO_2 catalyst was 0.004, so this catalyst was deactivated later than other ones. The higher amount of k_d for the 20%Ni/γ-Al_2O_3 catalyst demonstrated a higher rate of deactivation for this composition. Hence, applying TiO_2 support for the active nickel phase enhanced the long-term stability of the Nickel catalyst.

The values predicted by the models were compared with the new data to evaluate the validity of the models. Figures 2-5 show the results of the validation. It is confirmed that the deactivation model of GPLE2 for 20%Ni/TiO_2 and the GPLE1 model for the other catalysts are more appropriate.

Table 3. Deactivation Model Parameters for the Supported Nickel Catalysts

Catalyst	Order	k_d (min^{-1})	a_∞	R^2	R^2_{adj}
20%Ni/SiO_2	1	0.020	0.06	0.99	0.99
20 %Ni/α-Al_2O_3	1	0.016	0.066	0.99	0.99
20%Ni/γ-Al_2O_3	1	0.05	0.042	0.99	0.99
20%Ni/TiO_2	2	0.004	0.2	0.97	0.97

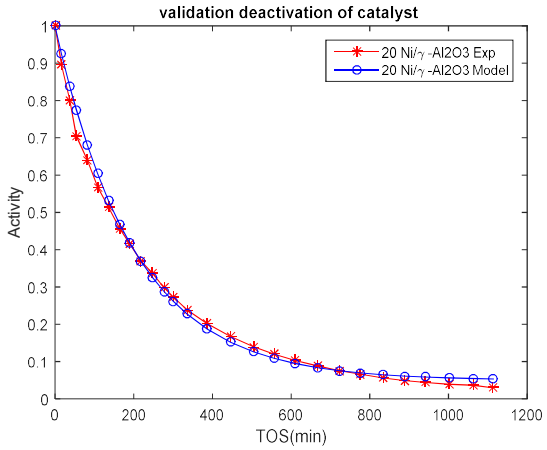


Fig. 2. Validation graph for the $20\%Ni/\gamma - Al_2O_3$ catalyst using the first-order GPLE model.

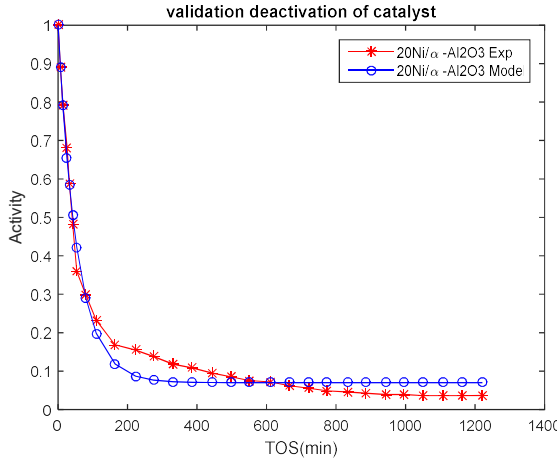


Fig. 3. Validation graph for the $20\%Ni/\alpha - Al_2O_3$ catalyst using the first-order GPLE model.

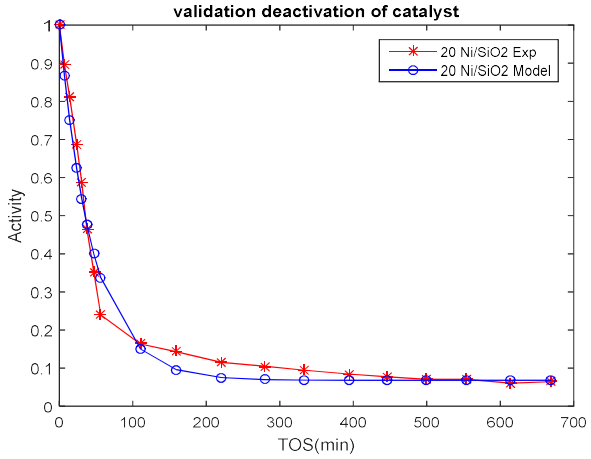


Fig. 4. Validation graph for the $20\%Ni/SiO_2$ catalyst using the first-order GPLE model.

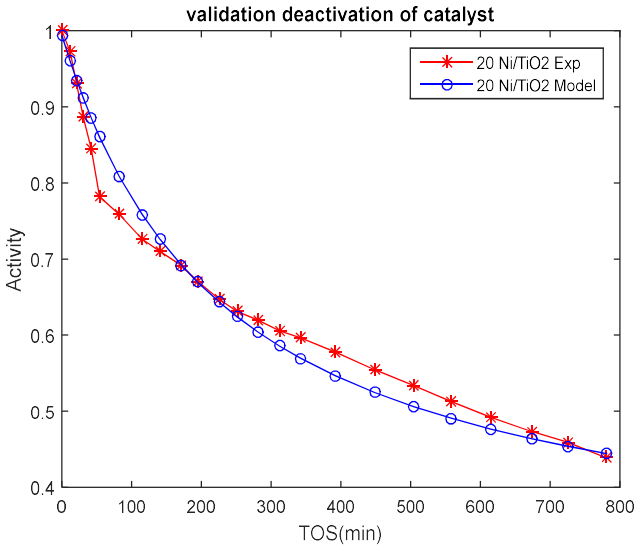


Fig. 5. Validation graph for the $20\%Ni/TiO_2$ catalyst using the second-order GPLE model.

Table 3 shows the mean particle sizes of nickel in the catalysts after 24 h of time on stream. The $20\%Ni/TiO_2$ and $20\%Ni/\alpha-Al_2O_3$ catalysts with maximum initial particle sizes loosed the least surface area. The mean particle size of nickel in the $20\%Ni/\gamma-Al_2O_3$ catalyst is greater than $20\%Ni/SiO_2$ one. It seems that sintering is dependent mainly on the initial sizes of the crystals.

Table 4 indicates that the mechanisms of catalyst deactivation in this study are sintering. Moreover, the sintering rate depended on the support type and initial values of nickel crystal sizes. The TiO_2 support had a 31% loss of surface area and 44% growth of nickel crystal size. Deactivation modeling demonstrated that the deactivation rate constant (K_d) for the TiO_2-supported nickel catalyst was lower than the other ones, indicating that this catalyst was deactivated later with a lower deactivation rate. For the catalyst with γ-Al_2O_3 support, crystal growth and the loss of surface area were 340% and 77%, respectively. Therefore, the γ-Al_2O_3-supported nickel catalyst had faster sintering rates.

CONCLUSION

The deactivation model is based on the mathematical description of catalyst stability. Determining the long-term stability of a catalyst is a time-consuming and costly procedure. Artificial Neural Network (ANN) is economically advantageous for accurate data extrapolation and predicting the long-term behavior of expensive industrial catalysts. In this research, the effects of support types on the stability of a nickel catalyst in a fixed-bad reactor were evaluated using general power-law expressions (GPLE) and Artificial Neural Networks (ANN). Model determination with ANN showed that for the 20%Ni/TiO_2 catalyst, the second-order GPLE model, and the other catalysts, the first-order GPLE model was in better agreement with experimental data. The deactivation constant (k_d) was higher for the 20%Ni/γ-Al_2O_3 catalyst. As a result, the 20%Ni/γ-Al_2O_3 catalyst had lower stability. The small k_d for the 20%Ni/TiO_2 catalyst showed that the Ni catalyst stability was higher on the TiO_2 support in the fixed-bed reactor.

ACKNOWLEDGMENT

The authors would like to acknowledge the financial support from the University of Sistan and Baluchestan, Islamic Republic of Iran.

Table 4. Sintering of the Ni Particle [28]

Catalyst	$d(Ni^o)_{XRD}$ (nm)	$d(Ni^o)_{XRD}$ *after reaction* (nm)	*Crystal*[a] *growth*(%)	*Loss of Ni surface area*[b](%)
$20\%Ni/TiO_2$	25	36	44	31
$20\%Ni/\alpha-Al_2O_3$	25	39	56	36
$20\%Ni/SiO_2$	13	46	254	72
$20\%Ni/\gamma-Al_2O_3$	10	44	340	77

[a] *Calculated according to* $=(d(Ni^o)_{XRD}after\ reaction - d(Ni^o)_{XRD})/(d(Ni^o)_{XRD})$

[b] *Calculated from the XRD measurements assuming spherical particles*

REFERENCES

[1] Tirado, A.; Ancheyta, J.; Trejo, F., Kinetic and reactor modeling of catalytic hydrotreatment of vegetable oils. *Energy & Fuels*, **2018**, *32*(7), 7245-7261.

[2] Sharma, Y. C., *et al*., Ethanol steam reforming for hydrogen production: Latest and effective catalyst modification strategies to minimize carbonaceous deactivation. *Renewable and Sustainable Energy Reviews*, **2017**, *74*, 89-103.

[3] Liu, Z., *et al*., Total methanation of syngas to synthetic natural gas over Ni catalyst in a micro-channel reactor. *Fuel*, **2012**, *95*, 599-605.

[4] Abbaslou, R. M. M.; Soltan, J.; Dalai, A. K., Iron catalyst supported on carbon nanotubes for Fischer-Tropsch synthesis: Effects of Mo promotion. *Fuel*, **2011**, *90*(3), 1139-1144.

[5] Schubert, M., *et al*., The Influence of the Pyrolysis Temperature on the Material Properties of Cobalt and Nickel Containing Precursor Derived Ceramics and their Catalytic Use for CO_2 Methanation and FischerTropsch Synthesis. *Catalysis Letters*, **2017**, *147*(2), 472-482.

[6] Schulz, H., Major and minor reactions in Fischer-Tropsch synthesis on cobalt catalysts. *Topics in Catalysis*, **2003**, *26*(1), 73-85.

[7] Amin, M., *et al*., Issues and challenges of Fischer-Tropsch synthesis catalysts. *Frontiers in Chemistry*, **2024**, *12*, 1462503.

[8] MohammadRezapour, M.; Mirzaei, A. A.; Zohdi-Fasaei, H., Optimizing the preparation conditions of silica supported Fe-Co-Ce ternary catalyst for the fixed-bed Fischer-Tropsch synthesis: Taguchi experimental design approach. *Physical Chemistry Research*, **2018**, *6*(2), 387-397.

[9] Teimouri, Z.; Abatzoglou, N.; Dalai, A. K., Kinetics and selectivity study of Fischer-Tropsch synthesis to C_{5+} hydrocarbons: a review. *Catalysts*, **2021**, *11*(3), 330.

[10] Zhang, Z., *et al*., Preparation, modification and development of Ni-based catalysts for catalytic reforming of tar produced from biomass gasification. *Renewable and Sustainable Energy Reviews*, **2018**, *94*, 1086-1109.

[11] Li, H., *et al*., Nickel catalysts supported on ordered mesoporous SiC materials for CO_2 reforming of methane. *Catalysis Today*, **2018**, *317*, 76-85.

[12] Zhang, X., *et al*., Carbon dioxide reforming of methane over Ni nanoparticles incorporated into mesoporous amorphous ZrO_2 matrix. *Fuel*, **2015**, *147*, 243-252.

[13] Su, Y. -Q., *et al*., Stable Pd-doped ceria structures for CH_4 activation and CO oxidation. *ACS Catalysis*, **2018**, *8*(1), 75-80.

[14] Eltejaei, H., *et al*., Methane dry reforming on $Ni/Ce_{0.75}Zr_{0.25}O_2$–$MgAl_2O_4$ and $Ni/Ce_{0.75}Zr_{0.25}O_2$–γ-alumina: effects of support composition and water addition. *International Journal of Hydrogen Energy*, **2012**, *37*(5), 4107-4118.

[15] Nurunnabi, M., *et al*., Performance of NiO-MgO solid solution-supported Pt catalysts in oxidative steam reforming of methane. *Applied Catalysis A: General*, **2005**, *292*, 272-280.

[16] Xu, L.; Song, H.; Chou, L., Ordered mesoporous MgO-Al_2O_3 composite oxides supported Ni based catalysts for CO_2 reforming of CH_4: Effects of basic modifier and mesopore structure. *International Journal of Hydrogen Energy*, **2013**, *38*(18), 7307-7325.

[17] Liu, D., *et al.*, Carbon dioxide reforming of methane to synthesis gas over Ni-MCM-41 catalysts. *Applied Catalysis A: General*, **2009**, *358*(2), 110-118.

[18] da SQ Menezes, J. P.; Manfro, R. L.; Souza, M. M., Hydrogen production from glycerol steam reforming over nickel catalysts supported on alumina and niobia: Deactivation process, effect of reaction conditions and kinetic modeling. *International Journal of Hydrogen Energy*, **2018**, *43*(32), 15064-15082.

[19] Barrientos, J., *et al*., Deactivation of $Ni/\gamma\text{-}Al_2O_3$ catalysts in CO methanation: Effect of Zr, Mg, Ba and Ca oxide promoters. *Topics in Catalysis*, **2017**, *60*(17-18), 1276-1284.

[20] Oboh, I. O.; Amaraegbu, O. R., Hydrocarbon Distribution of a Catalytic Process-The Fischer-Tropsch Synthesis. *American Journal of Chemistry and Application*, **2018**, *5*(1), 1-7.

[21] Olesen, S. E., *et al*., Deactivating carbon formation on a Ni/Al_2O_3 catalyst under methanation conditions. *The Journal of Physical Chemistry C*, **2017**, *121*(29), 15556-15564.

[22] Wang, J., *et al*., Deposition of carbon species on the surface of metal: As a poison or a promoter for the long-

term stability of Ni/SiO_2 methanation catalyst? *Chemical Engineering Journal*, **2017**, *322*, 339-345.

[23] Zhao, A., *et al*., Ni–Al_2O_3 catalysts prepared by solution combustion method for syngas methanation. *Catalysis Communications*, **2012**, *17*, 34-38.

[24] Dowlati, M.; Siyavashi, N.; Azizi, H. R., Sintering and Coking: Effect of Preparation Methods on the Deactivation of Co-Ni/TiO_2 in Fischer-Tropsch Synthesis. Arabian Journal for Science & Engineering (Springer Science & Business Media BV), **2018**. *43*(5).

[25] Van de Loosdrecht, J., *et al*., Metal-support interaction: titania-supported and silica-supported nickel catalysts. *Journal of Catalysis*, **1997**, *170*(2), 217-226.

[26] Shiva, M., *et al*., The application of hybrid DOE/ANN methodology in lumped kinetic modeling of Fischer-Tropsch reaction. *Fuel processing technology*, **2013**, *106*, 631-640.

[27] Ghofran Pakdel, M. *et al*., Neural Computing Strategy for Predicting Deactivation of Fischer-Tropsch Synthesis With Different Nickel Loadings. *Catalysis Letters*, **2019**, *149*(9), 2444-2452.

[28] Barrientos, J., *et al.*, Deactivation of supported nickel catalysts during CO methanation. *Applied Catalysis A: General*, **2014**, *486*, 143-149.

[29] Mansouri, S., *et al*., Effect of mass transfer on the deactivation model and GPLE parameters of Co/γ-Al_2O_3 catalysts in the Fischer Tropsch synthesis. *International Journal of Hydrogen Energy*, **2022**, *47*(75), 32031-32038.